LANGMUIR

pubs.acs.org/Langmuir Article

High Yield Au Nanorods Synthesis: Investigation of the Synthesis Parameters Tunability by Statistical Methods

Antonin Engel, Fabien Drault, Sophie Madeleine Demoustier-Champagne,* and Sophie Hermans*

Cite This: *Langmuir* 2025, 41, 15805−15818 Read Online

ACCESS | Metrics & More | Article Recommendations | Supporting Information

ABSTRACT: Gold nanorods are well-known for their localized surface plasmon resonance (LSPR) properties, which are sensitive to both their size and morphology. This LSPR effect, combined with their absorption ranging from the visible to the infrared portion of light, makes them particularly suitable for applications in fields such as photocatalysis, photovoltaics, biosensing, and medical imaging. Traditionally, their synthesis has been based on a seed-mediated method with the use of ascorbic acid as a mild reducing agent. In this work, hydroquinone is used as a reducing agent to achieve nearly quantitative yield in terms of gold consumption. Using a customized design of experiment, the present study explores the influence of seed, silver nitrate, cetyltrimethylammonium bromide (CTAB), hydroquinone, and gold precursor concentrations on the second LSPR wavelength value, linked to the rod aspect ratio (AR). Statistical analysis of the results revealed multiple significant quadratic effects and interactions, notably between CTAB and silver nitrate, indicating the formation of a complex between these two components that results in anisotropic growth. The predictive power of the developed model was investigated and validated by its accuracy in predicting, for new conditions, the plasmonic properties of nanorods with a well-controlled AR. This comprehensive understanding of the tunability and mechanism of the process provides valuable insights into optimizing the production of gold nanorods with desired properties for various applications. To this end, a web application was developed to enable any researcher to freely access the model designed in this work and choose the optimal experimental conditions for synthesis.

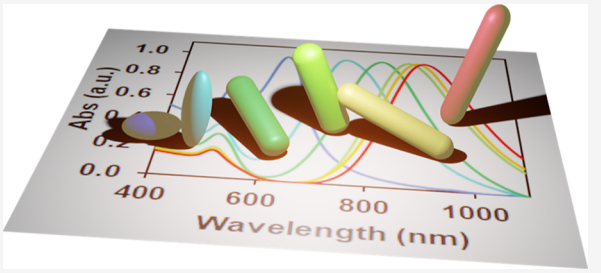

INTRODUCTION

Plasmonic particles are able to interact with light at specific wavelengths by exciting the coherent oscillation of their free electrons. This phenomenon is called localized surface plasmon resonance (LSPR) and only occurs when the frequency of the incoming electromagnetic wavelength matches that of the oscillating free electrons, which is only possible for nanometer-sized particles.[1,2] This unique property is shared by a large number of different metals, the most performant in this respect being gold, silver, and copper nanoparticles.[1−3] Indeed, these particles can absorb visible light (Ag, Au, Cu) or even near-infrared light (Au, Cu), thanks to their LSPR bands, paving the way for the use of solar energy to excite them.[2] Gold nanoparticles (NPs) are the most interesting due to their higher resistance to oxidation and atmospheric stability.[4] Moreover, the plasmonic response of a metallic NP is really sensitive not only to its size but also to its morphology.[5] For gold, a wide variety of morphologies have been studied: nanospheres,[6] nanotriangles,[7] nanostars,[8] nanorods (NRs).[9] Among all these possible morphologies, nanorods have attracted enormous attention over the last two decades due to their tunable aspect ratio (AR), i.e., the ratio between the longitudinal and transversal dimensions of the rod, leading to two LSPR modes, i.e., two absorbance bands in the visible-infrared range. It is now well established that the position of the second plasmonic peak (λ_2) and the AR of the obtained gold nanorods are linearly related.[10] By compiling multiple results from the literature, the following equation was established[11]

$$\lambda_2 = 95\mathrm{AR} + 420 \quad (1)$$

Therefore, by adjustment of the AR, it is possible to tune the absorption of Au NRs from visible to infrared. Thanks to their unique and exceptional plasmonic properties, gold nanorods have numerous applications in different fields, such as photocatalysis,[12] photovoltaics,[13,14] display technology,[15,16] therapy,[17,18] biosensors,[19,20] and medical imaging.[20,21]

The most widely used method for fabricating gold nanorods is the two steps seed-mediated synthesis, developed by Murphy et al. in 2001.[9,22] The first step consists of producing very small gold seeds (<5 nm) using a strong reducing agent ($NaBH_4$) in a micellar aqueous solution of $HAuCl_4$.[23] The second step requires the introduction of the seeds into a so-called "growth

Received: January 22, 2025
Revised: April 25, 2025
Accepted: April 30, 2025
Published: May 6, 2025

https://doi.org/10.1021/acs.langmuir.5c00326
Langmuir 2025, 41, 15805−15818

solution" containing a gold precursor ($HAuCl_4$), a surfactant (often CTAB) or surfactant mixture (CTAB and sodium oleate or CTAB, sodium oleate, and sodium salicylate) silver in the form of $AgNO_3$ and a mild reducing agent (ascorbic acid, hydroquinone, dopamine, ...).[10,24−27] Though ascorbic acid (A.A.) is the mild reducing agent most often reported in the literature, it is only able to reduce around 15% of the gold precursor into the metallic form.[24,28] However, it has been shown more recently that replacing A.A. by hydroquinone (HQ) leads to gold NRs with a nearly quantitative yield.[10]

Numerous studies have already been carried out to better understand and control the growth of Au nanorods by using this two-step seed-mediated method. However, in most of these studies, the authors have either varied a single synthesis parameter at a time, or studied several experimental factors, but without assessing the interactions between them.[10,25,29−33] Indeed, it has already been demonstrated that increasing the amount of seed can decrease or increase the AR[34] depending on the concentrations injected.[22,32,33,35] With regard to the concentrations of CTAB and $AgNO_3$ taken separately, their quadratic impact on the final AR is well-known in literature.[30,31] Finally, regarding the gold precursor ($HAuCl_4$), a quadratic influence has been found when used with A.A. as a mild reducing agent.[30]

There are, however, only a few examples of statistical studies of interactions between all the parameters, either through design of experiment (DOE) or machine learning methodology.[35−38] These studies, with A.A. as the reducing agent, revealed that the $NaBH_4$ concentration, the stirring speed (260−750 rpm) of the seed solution, and the aging time (1−5 h) of the seeds and growth solution (time between the addition of A.A. and the seeds: 1−30 min) are insignificant on the λ_2 position and therefore on the AR.[36]

On the contrary, it was found that the temperature (26−50 °C), amount of silver, A.A., and seeds had a significant impact, as well as the interaction between the amount of A.A. and silver and between the temperature and the amount of silver.[36] It was also shown that a strong interaction between silver and CTAB exists for both seed-mediated[35] and seedless synthesis methods.[39] This latter result is consistent with the claim in the literature that silver forms a complex with CTAB blocking specific crystallographic facets on growing seeds, resulting in anisotropic growth.[28,30,40,41] Finally, as with A.A. and $HAuCl_4$ together,[30] it would also be logical to find a strong interaction between the concentration of HQ and $HAuCl_4$, these two species reacting together in a redox-type reaction, but this has not yet been studied in detail. Furthermore, no statistical work is currently available to study all the chemical components of seed-mediated synthesis, i.e., CTAB, $AgNO_3$, $HAuCl_4$, HQ or A.A., and seeds.

Therefore, the main objective of the present contribution is to gain a comprehensive understanding of the impact of the amounts of all compounds used in seed-mediated synthesis and their interplay. This should enable better control of nanorod preparation and benefit all of the above-mentioned applications. This is particularly important when using HQ instead of A.A., given the difference in the yields between these two reducing agents. Therefore, a DOE was developed to study the impact of the concentration of seeds, silver nitrate, CTAB, HQ, and gold precursor and their potential interactions. Furthermore, our goal is to use this DOE to build a statistical model robust enough to become predictive. More specifically, we would like to be able to predict the plasmonic properties of synthesized gold NRs as a function of the concentration of the five different studied components present in the growth solution.

As this goal was achieved, this model is now available in the form of a web application at the following link: https://sites.uclouvain.be/cascados/, enabling either the λ_2 position to be predicted for given reactant concentrations or the reverse (i.e., the reactant concentrations required for obtaining a given λ_2). The developed model was validated by its ability to predict the plasmonic response of Au NRs grown under new conditions but also of gold nanorods synthesized by other research groups. This statistical model also provides pertinent insights into the mechanism of the growth reaction, confirming the previously reported impact of some factors but also highlighting new ones.

METHODS

Materials. Hexadecyltrimethylammonium bromide (CTAB, ≥98.0%), sodium borohydride ($NaBH_4$, ≥98.0%), silver nitrate ($AgNO_3$, ≥99.0%), and hydroquinone (HQ, 99%) were purchased from Sigma-Aldrich. Tetrachloroauric (III) acid ($HAuCl_4$, 99.999%) was purchased from Acros Organics. All chemicals were used as received without further purification.

Establishment of the Custom DOE. A custom DOE, aiming to optimize the Bayesian I-Optimality criterion, was designed using JMP Pro 17 software. This involves first the identification of the variables to study and their variation range. Then, a statistical model must be defined for these variables along with the number of experiments and eventual constraints.

Choice of the Parameters to Study. The most common synthesis method found in the literature to obtain gold NRs is the seed-mediated synthesis, which implies two steps. In the first one, small gold nuclei (seeds) are produced by the reaction of $HAuCl_4$ with $NaBH_4$. Then, in the second step, those seeds are grown in a growth solution made of $HAuCl_4$, CTAB, $AgNO_3$, and a mild reducing agent. Due to the difference in global yield from Au(III) to Au(0) when using A.A. (∼15%) or HQ (∼100%),[10,28] HQ has been selected as a mild reductor in this work.

The linear and quadratic influences of the seeds, HQ, CTAB, $AgNO_3$, and $HAuCl_4$ have been considered in the statistical study. A block variable of four experiments per block has also been included in the model to take into account the variability of the process from batch-to-batch (changes in ambient temperature, humidity in the air, stock solutions, ...). Moreover, the interactions of CTAB with $AgNO_3$, CTAB with $HAuCl_4$ and $HAuCl_4$ with HQ have been considered in the statistical model due to the documented formation of a complex between CTAB and $AgNO_3$, as well as between CTAB and $HAuCl_4$ and the redox reaction taking place between $HAuCl_4$ and HQ, respectively (see below Table 2).[29,42] However, other interactions such as the one between the seeds and CTAB, the seeds and $HAuCl_4$, ... have not been integrated because they are poorly or not at all reported in the literature but also to limit the number of experiments required to establish the statistical model.

Determination of the Variable Ranges. Each variable (seeds, $AgNO_3$, CTAB, HQ, and $HAuCl_4$) has been studied on three levels in order to consider their quadratic impact. The determination of the minimal and maximal levels (−1 and +1, respectively) is based on the concentrations found in the literature or in unpublished work of our lab for the seed-mediated synthesis of gold nanorods using HQ as a mild reducing agent (Table 1). The intermediate level is therefore set as the arithmetic mean of these two levels. The combination of all the variable ranges constitutes the design domain.

Calculation of the Custom DOE and Analysis of the Results Obtained. Once the model to be studied and the design domain have been defined, the number of experiments to be carried out need to be specified (24 here) as well as the number of repetitions (4 times) of the central point (the point at which all the variables are set at their 0 level, i.e., their intermediate level) of the entire domain. Then, the program outputs a list of 24 experiments to be carried out, divided into 6 blocks of 4 experiments. For each experiment carried out, the prepared

https://doi.org/10.1021/acs.langmuir.5c00326
Langmuir 2025, 41, 15805−15818

Table 1. Summary of the −1 and +1 Levels Values for the Different Parameters Included in the DOE

parameters	levels	
	−1	+1
CTAB (mM)	9.6[43]	96.0[43]
$AgNO_3$ (mM)	0.04[31]	1.45[41]
$HAuCl_4$ (mM)	0.46[41]	0.69
HQ (mM)	4.6[41]	19.8[31]
Seeds (μM)[a]	0.3[31,43]	7.1[10]

[a]For the seeds, the concentrations were calculated on the basis of the gold content, considering a 100% reduction yield from the Au(III) of the gold precursor to the Au(0) of the seeds.

nanoparticles are analyzed by UV−vis to determine the second plasmonic peak position (which is directly related to the AR), which is the response chosen to be studied. Finally, the 24 λ_2 measured are first modeled using a least-squares model considering the block variable as fixed and then using a mixed model considering the block variable as random. These analyses are carried out using JMP Pro 17 software.

Synthesis of Gold Nanorods. Each synthesis was performed using only fresh solutions of CTAB, $NaBH_4$, $AgNO_3$, and HQ.

Seed Solution. The seeds were prepared by adding 0.6 mL of freshly prepared cold $NaBH_4$ solution (10 mM) to a mixture containing both 0.12 mL of $HAuCl_4$ (14.5 or 1 mM) and 2.5 mL of CTAB (0.15 M). The seed solution was aged for 40 min at 25 °C before use.

Growth Solution. In the order of addition, a certain amount of mQ water (in order to reach a total volume of 10.2 mL), CTAB (0.15 M), and $HAuCl_4$ (14.5 mM) were mixed under stirring (350 rpm) in a 50 mL Erlenmeyer heated at 30 °C in an oil bath. Then, $AgNO_3$ (4, 15, or 20 mM) was added. Finally, the hydroquinone (0.1 M) was added 2 min before the addition of the seed solution. The solution changed from dark yellow to colorless with the addition of hydroquinone. The solution was aged for 24 h at 30 °C. The solution was analyzed by UV−vis spectrometry and then purified by centrifugation (ALC centrifuge PK 120, 9000 rpm, 30 min, RT, Corning 50 mL centrifuge tubes, CentriStar Cap). The supernatant was removed, and the deposit was redispersed in mQ water to reach a total volume of 25 mL. The volume of water, CTAB, $HAuCl_4$, $AgNO_3$, HQ, and seeds added is such that the final concentration in the growth solution is that indicated in Table S1.

Characterization Techniques. Transmission electron microscopy (TEM) images were collected on an LEO 922 Omega Energy Filter Transmission Electron Microscope operating at 120 kV and on a Thermo Fisher TALOS F200i Transmission Electron Microscope operating at 200 kV. Prior to analysis, samples were dispersed in water using ultrasonication if necessary. Then, a drop of the suspension was deposited on a C-flatTM thick grid (Standard 20 nm Carbon, 1.2 μm hole diameter, and 1.3 μm hole spacing with a 200-mesh copper grid, Protochips) before drying overnight. The AR was measured by TEM on the basis of 71 (7−112) particles averaged over 7 (4−12) images on average.

UV−vis spectra were obtained on a Shimadzu 1700 UV−vis spectrophotometer with quartz cuvettes. 500 μL of the as-synthesized gold nanoparticle suspensions were diluted in 1 mL of mQ water (18 mΩ) prior to the UV−vis absorption measurements. For stability analysis, nanorods were either centrifuged, with the supernatant replaced by mQ water and stored for 1 year in the fridge (5 °C) or stored without further purification at room temperature for 1 year.

RESULTS AND DISCUSSION

Establishment of Custom DOE. As mentioned in the Introduction section, according to the literature, seeds, hydroquinone, gold precursor, silver nitrate, and CTAB are expected to have a significant impact on the AR of gold NRs synthesized by the seed-mediated method.[10,22,26−32,36−37] We therefore designed a customized DOE that takes into account the influence of the concentration of each of these components on the resulting AR. To the best of our knowledge, this is the first time that the impact of all five components ($AgNO_3$, CTAB, $HAuCl_4$, HQ, and seed concentrations) involved in the seed-mediated synthesis of Au NRs is studied together using statistical tools. The various continuous numerical variables as well as the interactions included in the present customized DOE are summarized in Table 2.

Table 2. Continuous Variables and Interactions Integrated in the JMP Model

linear variables	quadratic variables	interactions
C $AgNO_3$	C $AgNO_3$ × C $AgNO_3$	C $AgNO_3$ × C CTAB
C CTAB	C CTAB × C CTAB	C $HAuCl_4$ × C CTAB
C seeds	C seeds × C seeds	C $HAuCl_4$ × C HQ
C $HAuCl_4$	C $HAuCl_4$ × C $HAuCl_4$	
C HQ	C HQ × C HQ	

This JMP-generated customized design comprises 24 experiments divided into 6 blocks of 4 experiments (Tables 3 and S1). The influence of the block variable is also studied and takes into account the process variability from batch to batch (stock solutions being renewed between each block). Finally, as output, the position of the second plasmonic peak (λ_2) was measured by UV−vis spectrometry for the 24 samples, after dilution of the NRs by a factor of 3 (Figure S1). In addition, for some of the samples, rod AR was measured by TEM microscopy (Figure S2). These results are also summarized in Table 3.

AR Determination. As mentioned in the Introduction section,[11] there is a linear relationship between the position of the second plasmonic peak and the AR of the gold nanorods. To confirm this, a simple linear regression between the AR and λ_2 was first used to fit the data acquired in the DOE (Figure 1). The following equation was obtained

$$\lambda_2 = 97\mathrm{AR} + 436 \quad (2)$$

This second equation ($R^2 = 0.97$), based solely on our own results, is very similar to the one proposed by Huang et al.[11] (eq 1), confirming that the linear relationship can indeed be extended to our results using this model. This linear relationship between λ_2 and AR is very useful as it makes it possible to easily and quickly obtain an estimation of the AR of Au NRs by UV−vis spectroscopy rather than having to resort systematically to a much more expensive and time-consuming characterization by TEM. Consequently, the following discussion relies solely on the observation of variations in the position of the second plasmonic peak to draw direct conclusions about the AR of the prepared nanorods.

Prediction of the λ_2 Position. The results obtained from the 24 experiments carried out under the conditions described in Table 3 were used to build a statistical model predicting the position of the second plasmonic peak and including the determination of all of the interactions listed in Table 2.

Two options are conceivable for building the model:

(i) Consider the blocks as categories of a fixed variable, which enables them to be compared, but limits the generalization of results to these blocks only.

(ii) Consider blocks as emanating from a random variable. In this case, the comparison of blocks is no longer relevant, and the generalization can be made to any other set of blocks, and hence to any other experiment.

This model first considers the block as a "fixed" variable.

https://doi.org/10.1021/acs.langmuir.5c00326
Langmuir 2025, 41, 15805−15818

Table 3. Second Plasmonic Peak Position[a] and Rod Aspect ratio[b] as Function of Variable Concentrations for the 5 Components Studied in the DOE

Block	$AgNO_3$ (mM)	$HAuCl_4$ (mM)	CTAB (mM)	HQ (mM)	Seeds (μM)	λ_2[(a)] (nm)	AR[(b)]
1	1.45	0.57	96.0	19.8	7.1	926	5.4
1	0.04	0.69	96.0	12.2	3.7	547	1.0
1	1.45	0.46	52.8	4.6	3.7	985	/
1	0.74	0.69	9.6	4.6	0.3	534	1.0
2	1.45	0.46	9.6	12.2	7.1	670	2.7
2	0.74	0.57	52.8	12.2	3.7	908	/
2	0.04	0.69	9.6	19.8	3.7	680	2.8
2	0.04	0.57	96.0	4.6	0.3	539	1.0
3	0.04	0.69	52.8	4.6	7.1	603	/
3	1.45	0.46	96.0	12.2	0.3	924	/
3	0.74	0.46	9.6	19.8	3.7	681	2.6
3	0.74	0.57	52.8	12.2	3.7	910	/
4	1.45	0.69	96.0	4.6	3.7	849	/
4	1.45	0.57	9.6	19.8	0.3	530	/
4	0.74	0.46	96.0	4.6	7.1	1071	/
4	0.04	0.46	52.8	19.8	0.3	720	/
5	1.45	0.69	52.8	19.8	7.1	858	3.7
5	0.04	0.46	96.0	19.8	3.7	647	/
5	0.74	0.57	52.8	12.2	3.7	908	4.9
5	0.04	0.46	9.6	4.6	0.3	701	3.0
6	0.74	0.69	96.0	19.8	0.3	963	5.1
6	1.45	0.69	9.6	4.6	3.7	600	/
6	0.04	0.57	9.6	12.2	7.1	683	/
6	0.74	0.57	52.8	12.2	3.7	921	/

[a]λ_2 determined by UV−vis spectrometry. [b]AR determined from TEM images.

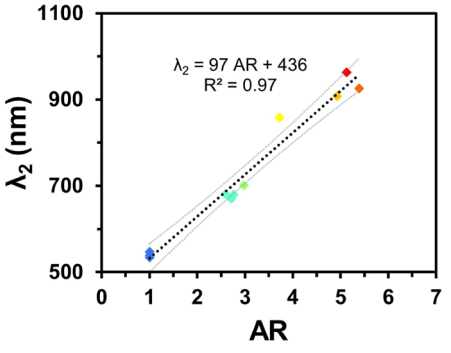

Figure 1. Plot of λ_2 (determined by UV−vis) versus AR (determined by TEM) for all the samples characterized by both UV−vis spectrometry and TEM microscopy. The lines in gray correspond to the upper and lower 95% confidence hyperbolas. The colors of the data point correspond to the λ_2 values.

To assess the significance of the various parameters studied, a *P*-value was calculated for each of them, a *P*-value <0.05 meaning that the studied variable is significant. This model has a R^2 of 0.99 and an adjusted R^2 (R_{adj}^2) of 0.93. This first model (fixed model), consisting of fixed variables only, highlights the nonsignificance of the "block" variable (*P*-value >0.05), which is related to the variability of the batch-to-batch process (Table 4, second column).

Table 4. *P*-Values of the Various Parameters Included in the Fixed and Mixed Models, as Well as the R^2 and R_{adj}^2 of the Two Models

models	fixed model	mixed model
R^2	0.99	0.98
R_{adj}^2	0.93	0.96
parameters	*P*-values	*P*-values
CTAB (mM)[a]	0.00058	0.00035
$AgNO_3$ (mM) × CTAB (mM)	0.00128	0.00079
$AgNO_3$ (mM)	0.00188	0.00119
$AgNO_3$ (mM) × $AgNO_3$ (mM)	0.00286	0.00181
$HAuCl_4$ (mM)	0.00535	0.00462
CTAB (mM) × CTAB (mM)	0.00575	0.00515
$HAuCl_4$ (mM) × HQ (mM)	0.00671	0.00299
seeds (mM)	0.0479	0.04404
seeds (mM) × seeds (mM)	0.15056	0.14967
block	0.15465	
$HAuCl_4$ (mM) × $HAuCl_4$ (mM)	0.19839	0.25617
CTAB (mM) × $HAuCl_4$ (mM)	0.51559	0.49523
HQ (mM) × HQ (mM)	0.81869	0.86328
HQ (mM)	0.88518	0.88016

[a]In bold, the significant parameters with a *P*-value <0.05.

This makes it possible to establish a second model with the "block" variable considered as random (Table 4, third column) so that the predictive potential of the model can be extended to all experiments, regardless of the batch from which they originate. This generalization of the model is a very important step and makes it predictive for new experiments, no matter when they are carried out. This mixed model has a R^2 of 0.98 and a R_{adj}^2 of 0.96. The R^2 value is close to 1, demonstrating the model's effectiveness in describing the relationship between the variables. In addition, the R_{adj}^2 value is close to that of R^2, meaning that the 14 variables included in the model do not lead to significant overfitting.

In addition, the graph in Figure 2, showing observed λ_2 versus predicted λ_2, highlights the closeness between observed and model-predicted values, with no experiment considered outliers. The plot of λ_2 residuals versus predicted λ_2 and the optimized regression equation are also available in the Supporting Information (Figure S3 and eq S1).

The reproducibility of the process was assessed by repeating the center point of the model 4 times (with a 0 level for all variables studied), leading to a λ_2 position equal to 912 nm on average with a narrow standard deviation of 6 nm (Table S2). Consequently, the synthesis of gold NRs carried out in this work can be considered to be highly reproducible.

Further statistical analysis of this second model reveals that 8 variables (in bold in Table 4) out of the 14 included in the model are significant. The *P*-values of those variables underline the huge linear and quadratic effects of both CTAB and $AgNO_3$, as well as their strong interaction. This finding is in good agreement with previously reported results and provides further

https://doi.org/10.1021/acs.langmuir.5c00326
Langmuir 2025, 41, 15805−15818

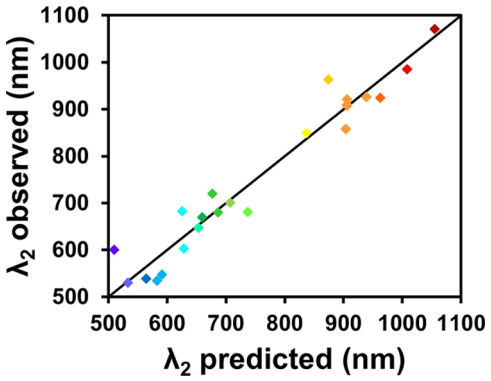

Figure 2. Observed by the predicted plot of the λ_2 position. The black line is a virtual line corresponding to perfect alignment between observed and predicted values. The colors of the data points correspond to the λ_2 values as visual illustration for the wide range of wavelengths explored.

evidence for the existence of a complex formed between silver and CTAB, formerly deduced from XPS data.[41] $HAuCl_4$ concentration is also significant but only linear. This result follows the same trend as observed by Nikoobakht and El-Sayed et al. up to 1 mM with A.A. as the reducing agent in the growth solution. In the same work, a quadratic trend was observed but with a noticeable inflection above 1 mM.[30] In addition, there is a strong interaction between the concentrations of $HAuCl_4$ and HQ, which is not surprising, given the reaction that occurs between these two species in solution. On the other hand, the interaction between $HAuCl_4$ and CTAB is not significant, which does not necessarily contradict the formation of a complex between these two species, but suggests that the effect of this complex is negligible on rod growth compared to other factors. Finally, seed concentration is significant but only linear.

Based on the model developed and the effect of the various variables studied, one way to tune the position of the second plasmonic peak (and therefore the AR) over a wide range (~700−900 nm with the parameters fixed in Figure 3, see Figure S4 for all the prediction profilers) is to adjust the concentration of silver nitrate or CTAB in solution. However, as these two variables have a strong quadratic relationship with the λ_2 position, a small error in their experimental concentration can lead to a significant inaccuracy in the obtained peak position (Figure 3A,B,E). In addition, it is important to consider that increasing $AgNO_3$ concentration has been shown to have a positive impact on morphological yield up to a certain critical value where its impact becomes negative (leading to more cubic and spherical impurities).[44] This tendency may explain the broader transversal absorption peak and thus the lower morphological purity for DOE-3, DOE-5, DOE-10, DOE-13, DOE-17, and DOE-22 (Figure S1). Furthermore, when the CTAB concentration is at its maximum (96 mM), i.e., for DOE-1, DOE-2, DOE-8, DOE-10, DOE-13, DOE-15, DOE-18, and DOE-21, the first absorption peak of rods is in most of the samples relatively broad, indicating also a higher level of morphological impurities, namely nanospheres (Figure S1).

Therefore, to obtain highly pure rods with predictive accuracy, we suggest targeting concentrations that are not too close to the extremes studied in this paper for both CTAB and $AgNO_3$. For this purpose, we have developed a web application (https://sites.uclouvain.be/cascados/) that allows the prediction of multiple combinations of concentrations giving the same λ_2. There, the operator has the choice between several conditions and can select the most favorable one according to the considerations just discussed.

In contrast, changing the $HAuCl_4$ concentration (Figure 3C) induces mostly linear changes in the λ_2 position, limiting the impact of an error in the experimental concentration without any visible impact on the sample purity. This gain in precision comes at a price as the range in which tuning is possible this way is narrower (900−1000 nm with the parameters set, as shown in Figure 3).

The stability of the synthesized nanorods was also studied. To investigate this, we compared the UV−vis absorption spectra directly after synthesis, after centrifugation (to discard the supernatant and replace it with mQ water) and 1 year of refrigerated storage (5 °C), and 1 year later without centrifugation and storage at room temperature (Figure S5 and Table S3). Regardless of storage conditions, a slight blue-shift of λ_2 was observed in most cases, in line with the stability and reshaping of nanorods toward nanospheres, as observed previously in the literature.[10] However, centrifugation, together with refrigerated storage, proved to be the best option. Indeed, the ratio of the two plasmonic peaks ($A_{\lambda 2}/A_{\lambda 1}$) is similar or even better (probably thanks to the purification centrifugation step) than that measured initially, whereas room temperature storage leads to a drastic decrease in this ratio. The full width at half-maximum (fwhm) of UV−vis peaks was also measured. Overall, whatever the storage conditions, the fwhm remained stable or slightly lowered over time. Regarding this latter effect, it is probably linked to the blue-shift observed over time, reflecting a remodeling of nanorod morphology and hence a change in the AR distribution.

Validation of the Model. In order to validate the model developed to predict the position of λ_2, 10 additional experiments were carried out. New combinations of $HAuCl_4$, seeds, HQ, $AgNO_3$, and CTAB concentrations were implemented in the model to predict the expected position of the second plasmonic peak. The resulting Au NRs were analyzed by UV−vis spectrometry and TEM microscopy (Figure 4 and Table 5).

All 10 measured λ_2 peak positions lie within the 95% prediction interval given by the model (see Figure S6 for UV−vis spectra). This 95% prediction interval means that there is only a 5% probability that the result of the experiment lies outside this prediction interval.

The experiments carried out show that this model can be used to predict and obtain rods with an extended range of λ_2 values (here from 604 to 1047 nm) by changing the concentration of the 5 reagents studied in this work.

Moreover, for experiments 1, 2, 4, 5, 6, 8, and 9, the observed value is very close to the predicted value, with a maximum deviation from the model of 37 nm for the ninth experiment. Only the experiments numbered 3, 7, and 10 differ further from the predicted value, with a deviation of 56, 50, and 71 nm, respectively. This latter result can be explained by the concentrations used for this synthesis, that were chosen to obtain the maximal value for λ_2, within the studied range of the DOE. This specific restriction requires the use of $HAuCl_4$ (−1) and HQ (−1) concentrations at their lowest level, as well as $AgNO_3$ and CTAB values close to their maximum (+1) level. Consequently, it is not surprising that the model performs less poorly in predicting λ_2 under these extreme conditions. Nevertheless, the observed value lies within the 95% prediction interval given by the model. Furthermore, using eq 2, the predicted AR was calculated on the basis of the observed λ_2

https://doi.org/10.1021/acs.langmuir.5c00326
Langmuir 2025, 41, 15805−15818

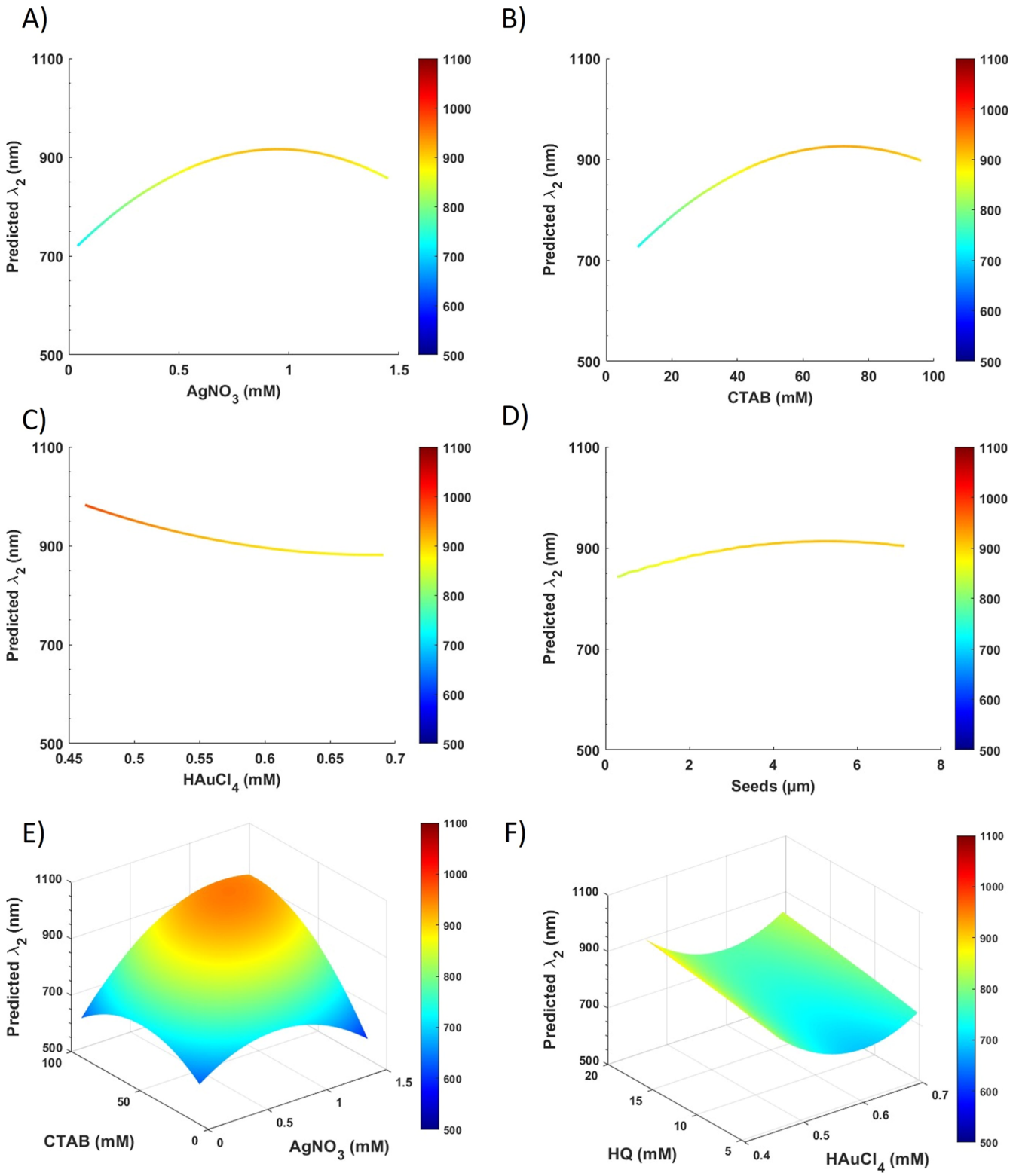

Figure 3. Prediction profilers of λ_2 position as a function of (A) $AgNO_3$, (B) CTAB, (C) $HAuCl_4$, (D) seeds, (E) $AgNO_3$ × CTAB, and (F) $HAuCl_4$ × HQ concentrations. For each surface profiler, the other parameters are set to their intermediate value (level 0).

values (Table 5). The observed and predicted AR values are close for all validation experiments, with the exception of the eighth, with a larger deviation of 1.3 in terms of AR.

To illustrate the detrimental effect of CTAB at high concentration, experiment 3 was carried out with the highest CTAB concentration (96.0 mM), with a predicted λ_2 around 800 nm (788 nm). Indeed, we can see that the first absorption peak is greatly broadened, which means that there is definitely a loss of morphological purity, as the first absorption peak overlaps with the one associated with nanospheres (Figure S6C). Those spherical impurities are also visible on the TEM image of VDOE-3 (Figure 4). On the other hand, if we lower the CTAB

https://doi.org/10.1021/acs.langmuir.5c00326
Langmuir 2025, 41, 15805−15818

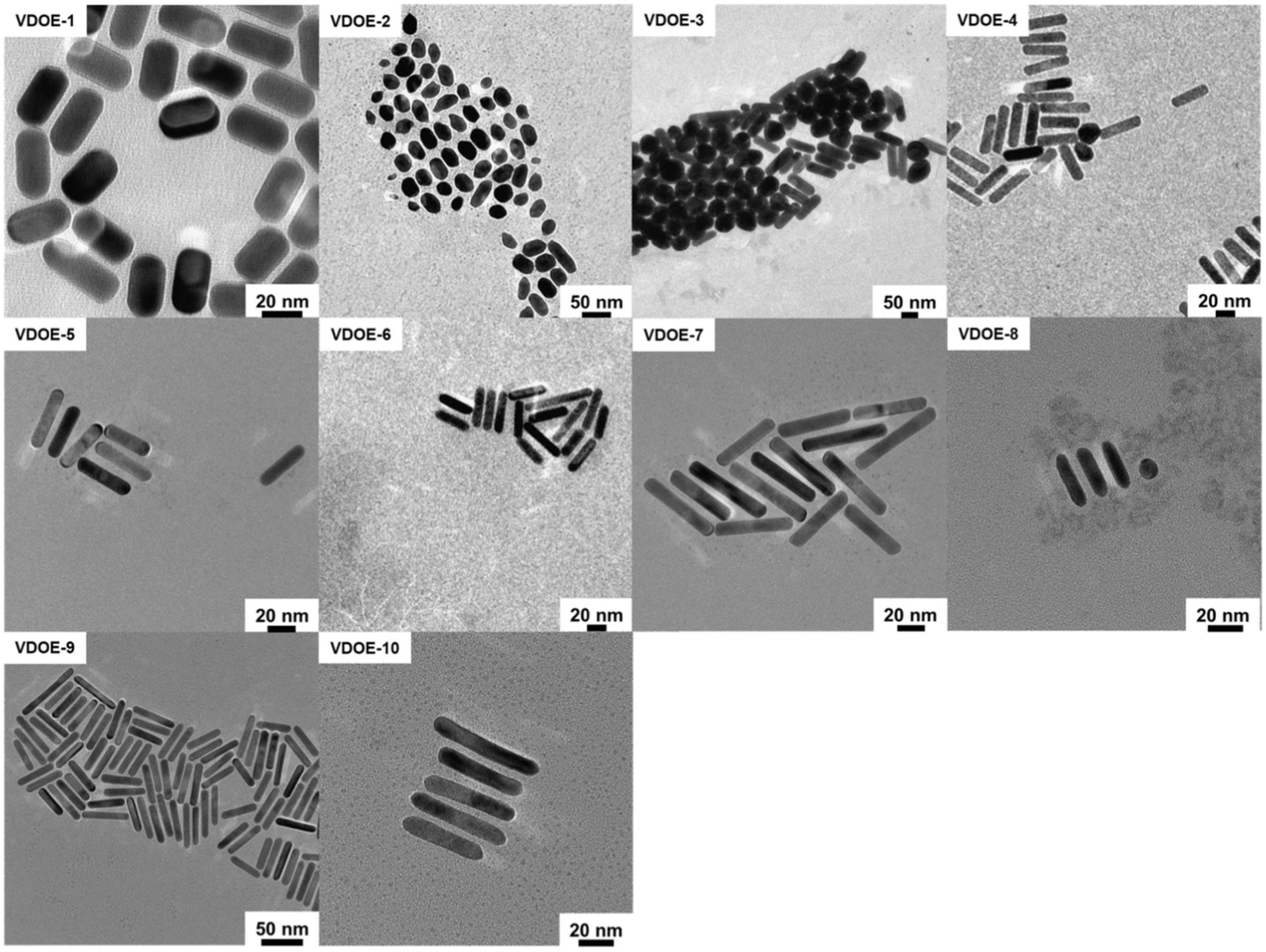

Figure 4. TEM images of the Au NRs obtained for the 10 validation experiments (noted VDOE-1, 2, 3, 4, 5, 6, 7, 8, 9, and 10).

Table 5. Predicted and Observed λ_2 Peak Positions Depending on the Conditions Set[a]

#	$AgNO_3$ (mM)	$HAuCl_4$ (mM)	CTAB (mM)	HQ (mM)	seeds (μM)	predicted[b] λ_2 (nm)	observed[c] λ_2 (nm)	predicted[d] AR	observed[e] AR $\pm \sigma$
1	0.05	0.71	48.0	4.9	5.3	636 [555, 716]	604	1.7	1.9 ± 0.3
2	0.07	0.69	48.0	5.0	4.6	652 [582, 722]	656	2.3	1.7 ± 0.3
3	0.74	0.71	96.0	4.9	3.7	788 [693, 883]	844	4.2	3.2 ± 0.6
4	0.86	0.71	42.2	5.8	3.7	799 [718, 881]	811	3.9	4.1 ± 0.6
5	0.86	0.71	42.2	5.8	3.7	799 [718, 881]	813	3.9	4.0 ± 0.5
6	0.86	0.71	42.2	5.8	3.7	799 [718, 881]	829	4.1	3.9 ± 0.7
7	0.74	0.71	52.8	11.9	3.7	880 [791, 969]	930	5.1	5.4 ± 0.9
8	0.74	0.65	52.8	12.2	3.7	884 [825, 943]	900	4.8	3.5 ± 0.4
9	1.02	0.51	70.9	12.2	3.6	984 [930, 1038]	947	5.3	5.5 ± 0.8
10	1.21	0.46	93.2	4.6	5.2	1118 [1037, 1199]	1047	6.3	5.9 ± 0.7

[a]In brackets the 95% prediction intervals. [b]Predicted λ_2 based on the concentrations injected. [c]λ_2 measured via UV−vis spectrometry. [d]Predicted AR based on the λ_2 measured via UV−vis spectrometry. [e]AR measured via TEM.

concentration (42.2 mM) and use the inverse prediction model to establish conditions for having a λ_2 around 800 nm (799 nm), we obtain much more morphologically pure rods (see experiments 4, 5, and 6 on Figure S6D).

Furthermore, entries 4, 5, and 6 demonstrate (Table 5), in addition to the 4 replicates of the central point carried out for the construction of the model (Table S2), the reproducibility of the proposed synthesis protocol with a λ_2 of 818 ± 10 nm, an AR of 4.0 ± 0.1, a fwhm of 202 ± 10 nm, and a $A_{\lambda 2}/A_{\lambda 1}$ ratio of 3.1 ± 0.4.

As for the experiments conducted to build the model, the stability of the synthesized nanorods was studied for experiments 8, 9, and 10 (VDOE-8, 9, and 10). The same rationalization can be made, i.e., a blue-shift and a narrower fwhm over time whatever the storage conditions and a much better preservation of the plasmonic properties with centrifugation and refrigerated storage (5 °C).

Now that the model developed in this work has been validated, it is possible to go a step further and use it to predict the λ_2 positions of NRs synthesized by other research groups.

https://doi.org/10.1021/acs.langmuir.5c00326
Langmuir 2025, 41, 15805−15818

Table 6. Predicted (Using Our Model) and Observed λ_2 Peak Position (as Reported) Depending on the Conditions Set in the Publications[a]

$AgNO_3$ (mM)	$HAuCl_4$ (mM)	CTAB (mM)	HQ (mM)	Seeds (μM)	Predicted λ_2 (nm)	Observed λ_2 (nm)	Ref.
0.05	0.47	93.2	4.7	7.1	748 [671, 825]	560	10
0.15	0.47	93.2	4.7	7.1	799 [728, 870]	770	10
0.35	0.47	93.2	4.7	7.1	887 [820, 954]	1150	10
0.65	0.47	93.2	5.0	7.1	983 [916, 1049]	1130	10
0.65	0.47	93.2	13.0	7.1	918 [857, 978]	970	10
0.04	0.49	48.6	19.6	0.3	705 [638, 771]	660	31
0.06	0.49	48.4	19.5	0.3	713 [647, 778]	740	31
0.08	0.49	48.1	19.4	0.3	720 [656, 785]	800	31
0.08	0.49	9.6	19.4	0.3	624 [552, 696]	660	43
0.08	0.49	19.2	19.4	0.3	662 [598, 726]	690	43
0.08	0.49	57.6	19.4	0.3	721 [656, 785]	760	43
0.08	0.49	76.8	19.4	0.3	693 [633, 753]	710	43
0.08	0.49	96.0	19.4	0.3	627 [559, 694]	665	43

[a]In brackets the 95% prediction intervals.

For this purpose, only papers using the same synthesis method as presented here were selected, i.e., a seed-mediated synthesis with HQ as the mild reducing agent (Table 6).

Remarkably, the model effectively predicts the observed values for roughly 70% of the results listed in Table 6. In this regard, the values highlighted in green fall within the 95% prediction interval given by the model. Nevertheless, some values (highlighted in red) fall outside this prediction interval, which may be explained by slight modifications to the process by other experimenters in other research groups. For example, the order and timing of addition of the different reagents used in the synthesis of gold NRs have a significant impact on the λ_2 position obtained,[45] and these details are not always provided.

Thanks to the high reproducibility of the experiments and the excellent R^2_{adj} (0.96) of the mixed model, it can be considered a valuable tool for anyone using the protocol described in this work. Therefore, a web application has been developed and is available online (https://sites.uclouvain.be/cascados/) to predict λ_2 position as a function of $AgNO_3$, CTAB, $HAuCl_4$, HQ, and seed concentrations and vice versa.

Now that the predictive efficiency of the model developed in this work has been demonstrated for both our own syntheses and those of other groups, it is possible to use these results to gain a better insight into the mechanisms involved in the formation of gold NRs.

Au NRs Formation Mechanism. *Seeds.* Seeds can be considered as small gold nuclei (<5 nm), which serve as the starting point for anisotropic growth, yielding rod-shaped NPs.[23,46]

Two types of gold NRs can be produced depending on the seed synthesis conditions: (i) citrate-capped seeds (~3.5 nm) which will give penta-twinned NRs and (ii) CTAB-capped seeds (<2 nm) which will produce single-crystal NRs (Figure 5).[23,46,47] The first type of seeds is responsible for the formation of NRs with high ARs, but with a relatively low shape yield (around 30%), while the second provides much better shape control (90−99% purity) and allows ARs to be controlled over a wide range (1.5−8).[10,23,46,47] It should be noted that a seedless synthesis also exists but leads to a morphologically less pure product and is less reproducible.[46] Due to their better characteristics, only the CTAB-capped seeds were used in this work. As prepared, these single-crystal seeds exhibit {111} crystallographic facets. However, when the seeds are poured into the growth solution, they start to grow and at some point, a symmetry breaking occurs, transforming the single-crystal seeds into anisotropic nuclei with {110} and {100} facets.[28,30]

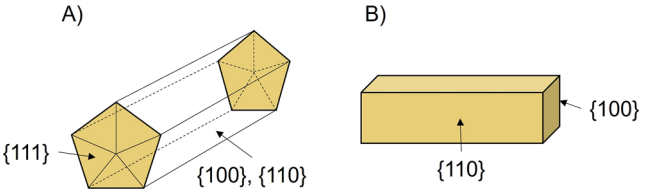

Figure 5. Schematic representation of the NRs obtained with (A) citrate-capped seeds and (B) CTAB-capped seeds. Adapted from ref 28. Copyright 2006 American Chemical Society.

Subsequently, these nuclei continue to grow anisotropically, thanks to the strong affinity of the complex formed by CTAB and silver for the less stable {110} facets, resulting in rod-shaped NPs.[28,48]

One way of modifying the AR via the seeds is to change their concentration in the growth solution. Indeed, it has been shown that increasing the seed concentration decreases the AR for concentrations ranging from $\sim 2 \times 10^{-4}$ μM to ~1 μM[32,33] and increases the AR for concentrations ranging from 0.3 μM to 10 μM.[35]

https://doi.org/10.1021/acs.langmuir.5c00326
Langmuir 2025, 41, 15805−15818

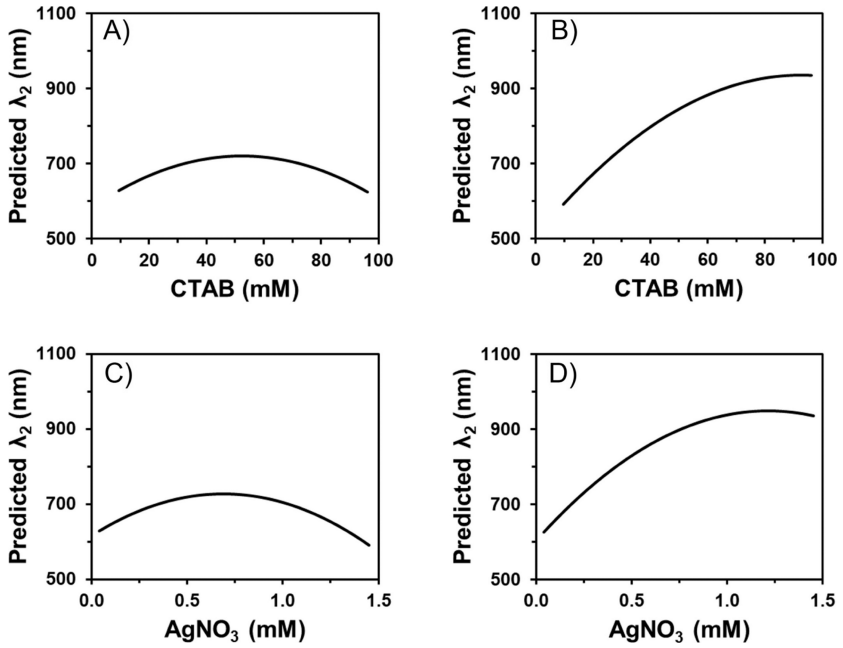

Figure 6. (A,B) Impact of the $AgNO_3$ fixed concentration (−1 and +1, respectively) on the curve linking CTAB and the predicted λ_2 position. (C,D) Impact of the CTAB fixed concentration (−1 and +1, respectively) on the curve linking $AgNO_3$ and the predicted λ_2 position. The other parameters are set to their intermediate value (0).

The model developed here is consistent with the trend observed in the literature for a 0.3 μM−10 μM concentration range[35] (the concentration range used in this study is 0.3−7.1 μM), i.e., increasing seed concentrations lead to an increase of the AR. This phenomenon can be explained by the fact that the number of seeds controls the quantity of rods obtained and therefore the amount of Au^{3+} deposited as Au^0 on each rod. Consequently, an increase in the number of seeds induces the production of rods with a smaller volume.[49] Experimentally, it has been observed that this decrease in volume is attributed to a decrease in length and width as the concentration of seeds increases, with a greater decrease in width than length, resulting in a larger AR.[30,35]

$AgNO_3$ and CTAB. Silver nitrate and CTAB are the two key components in the anisotropic growth that gives rise to NRs. In early studies of the mechanism of gold NRs formation, the influences of CTAB and silver nitrate were not fully understood and were sometimes decoupled.[30] Under the reaction conditions used in these studies, Ag^+ and Br^- concentrations were sufficiently high to cause the precipitation of AgBr ($K_s = 5 \times 10^{-13}$).[28,47] This precipitate was thought to deposit on the gold surface and to influence both {110} facet blocking and the termination step, i.e., the blocking of the {100} facets.[22,28,30]

Under potential deposition (UPD) of silver has also been proposed to explain the role of this metal.[23,28,46,47,50] This phenomenon is possible when the work function of the substrate (here, gold) is higher than that of the adlayer metal (here silver). For the Au−Ag system, the work function of gold is more than 0.5 eV higher than that of silver, making the UDP of silver favorable.[47] Consequently, the UPD takes place on both {110} and {100} facets, favoring the growth and termination of gold NRs, respectively.[28] More specifically, the UDP shift is greater on {110} facets, leading to preferential Ag^0 formation on the longitudinal dimension and poorer coverage on the tips.[23,47]

Regarding the surfactant, it is now generally accepted that CTAB forms a bilayer on the surface of gold NRs more selectively onto the {110} facets due to the greater interatomic Au−Au distance there compared with other facets.[48,50]

More recent studies have focused on the interaction between CTAB and silver nitrate, emphasizing the formation of a complex between these two compounds preferentially on the {110} facets. When CTAB and $AgNO_3$ are mixed in a ratio comprised between 1.5:1 and 2:1, the AgBr precipitate is transformed into an AgBr/CTAB complex with the empirical formula $C_{19}H_{42}NAgBr_2$.[40,45,51] Moreover, Amatori et al.[41] demonstrated the existence of the CTA^+---Br---Ag^+ coordination compound by XPS analysis on the surface of as-prepared gold NRs. The binding energies related to Br prove the existence of unimpacted Br^- bound to CTAB as well as less negatively charged Br^- ions, which are included in the sandwich structure formed by the CTA^+---Br^----Ag^+ complex. Their results also revealed that 90% of silver is present as Ag^+ and 10% as Ag^0 on the surface of gold NRs, tending to prove the existence of silver UPD.

The DOE developed here highlights a strong quadratic relationship between the concentration of $AgNO_3$ or CTAB and the obtained AR (Figure 3A,B). This trend has already been demonstrated by Nikoobakht and El-Sayed et al.[30] for $AgNO_3$ and by Morasso et al.[31] for CTAB, but without any rationalization of the quadratic curve observed, and especially of the negative influence of these two compounds at high concentrations. In the present work, we propose to rationalize the relationship by the formation of the $C_{19}H_{42}NAgBr_2$ complex. Two different regimes can be identified for both the $AgNO_3$ and CTAB concentrations effect (Figure 3A,B). At low concentrations of CTAB or silver nitrate, adding more CTAB/$AgNO_3$ leads to the formation of sufficient complexes and thus to better blocking of the {110} facets, resulting in stretched NRs. On the contrary, at higher concentrations of CTAB/$AgNO_3$, adding even more CTAB/$AgNO_3$ leads to the formation of much more complex and thus to a higher competition between binding on {110} facets compared to {100} facets, making the blocking of

https://doi.org/10.1021/acs.langmuir.5c00326
Langmuir 2025, 41, 15805−15818

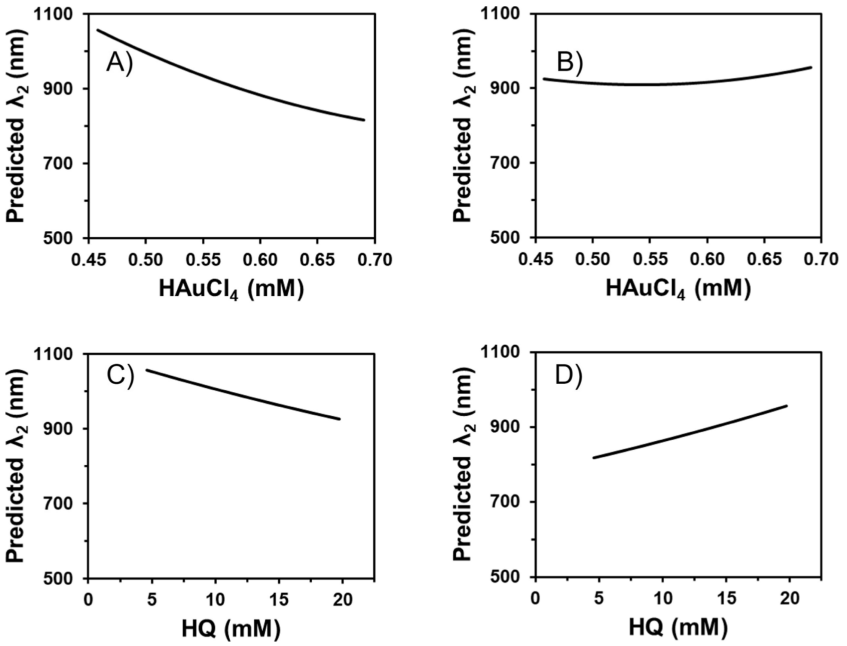

Figure 7. (A,B) Impact of the HQ fixed concentration (−1 and +1, respectively) on the curve linking $HAuCl_4$ and the predicted λ_2 position. (C,D) Impact of the $HAuCl_4$ fixed concentration (−1 and +1, respectively) on the curve linking HQ and the predicted λ_2 position. The other parameters are set to their intermediate value (0).

the {100} facets more favorable. This results in a faster termination rate of gold NRs growth compared to the low regime and hence lower ARs.

$AgNO_3$ and CTAB Interaction. This study is the second to provide statistical insights into the interactions between CTAB and $AgNO_3$, but this time with the use of HQ as a mild reducing agent and over a wider concentration range for both compounds, shifting to lower concentrations for CTAB (9.6–96 mM vs 40–120 mM) and higher concentrations for $AgNO_3$ (0.04–1.45 mM vs 0.02–0.2 mM).[35] At low concentrations of either CTAB or $AgNO_3$, increasing the concentration of the other partner ($AgNO_3$/CTAB) leads to two distinct regimes (Figure 6). The same rationalization as above can be made: (i) at low concentrations of CTAB/$AgNO_3$, adding more CTAB/$AgNO_3$ favors the blocking of the {110} facets, and (ii) at high CTAB/$AgNO_3$ concentrations, adding more CTAB/$AgNO_3$ makes the blocking of the {100} facets more favorable.

However, at high concentrations of CTAB or $AgNO_3$, two further contributions probably need to be added. First, the capping of the {100} facets by free CTAB micelles at high concentrations of CTAB and low concentrations of $AgNO_3$ resulting from a competition between CTAB and $C_{19}H_{42}NAgBr_2$ complex. Spalla et al.[51] already demonstrated the competition between these two species to cover the gold surface. Second, UPD of Ag^+ cations on the {100} facets occurs at high concentrations of $AgNO_3$ and low concentrations of CTAB.

$HAuCl_4$. When the gold compound, $HAuCl_4$, is in the presence of CTAB, ligand exchange between the chloride and bromide of CTAB occurs, yielding $[AuCl_{4-x}Br_x]^-$ anions.[45,52,53] Subsequently, these anions can form complexes with CTA^+ to form $CTA[AuCl_{4-x}Br_x]$ species, which will further be reduced to Au^0 to participate in the growth of the gold NRs.[28,33,46,51] In this study, no evidence of interactions between $HAuCl_4$ and CTAB concentrations could be highlighted from the statistical model (Table 4). As previously indicated, this does not necessarily mean that this interaction does not exist, but rather that it is very weak compared to the impact of the significant variables of the model, identified as $AgNO_3$ (linear and quadratic functions), CTAB (linear and quadratic functions), $HAuCl_4$ (linear function), and $AgNO_3$ × CTAB and $HAuCl_4$ × HQ concentrations. This is consistent with the assumption made by Jessl et al. that, upon addition of silver, and due to the higher affinity of halides for silver than for gold, the Au^+−CTAB complex is converted to the silver−CTAB complex.[44]

Nevertheless, the results obtained in this work allow us to conclude that increasing the $HAuCl_4$ concentration leads to an almost linear decrease in the AR of the gold NRs (Figure 3C). This result is consistent with the interplay between $HAuCl_4$ and hydroquinone (HQ), which serves as a mild reductor. Indeed, the reduction reaction of $HAuCl_4$ by HQ can be written into two steps[42,46]

$$3HQ + 3HAuCl_4 \rightarrow 3BQ + 3AuCl_2^- + 9H^+ + 6Cl^- \quad (3)$$

$$3AuCl_2^- \rightarrow 2Au^0 + AuCl_4^- + 2Cl^- \qquad K = 15.5 \times 10^7 \quad (4)$$

According to eqs 3 and 4, increasing $HAuCl_4$ concentration leads to an increase in both H^+ and $AuCl_4^-$ ions, which has a negative influence on the Au^0 formation. Therefore, by increasing the $HAuCl_4$ concentration, fewer $AuCl_2^-$ ions are produced, favoring the termination step over the growth step. This pH-dependent $HAuCl_4$/reductor interaction has already been documented in the literature for seedless gold nanospheres synthesis with HQ as a reductor.[42] Based on the model developed in this work, this interplay appears to be extendable to the seed-mediated synthesis of gold nanorods.

$HAuCl_4$ and HQ Interaction. This is the first time that the interaction between $HAuCl_4$ and HQ has been studied by using statistical tools. When the HQ concentration is set at its lowest value (4.6 mM), increasing the $HAuCl_4$ concentration results in a decrease in the obtained AR (Figure 7A). This result is

https://doi.org/10.1021/acs.langmuir.5c00326
Langmuir 2025, 41, 15805−15818

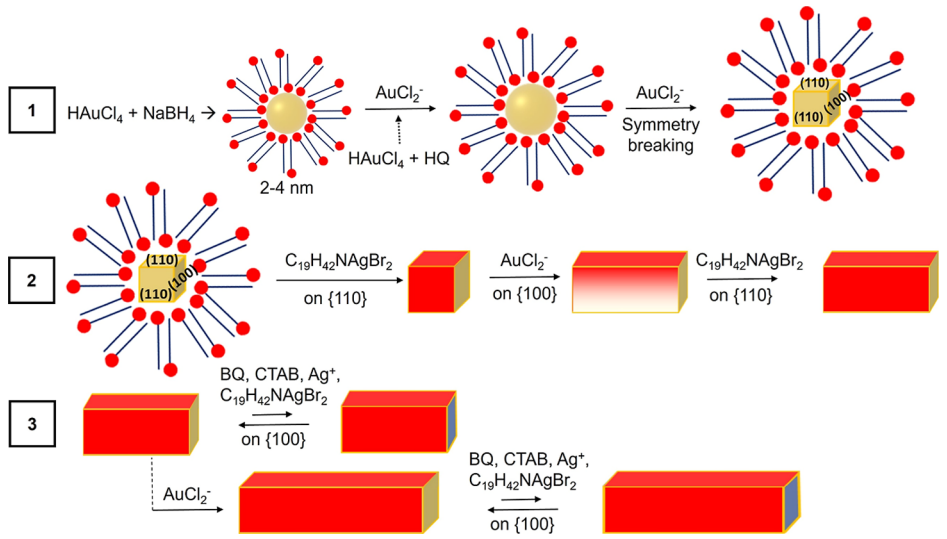

Figure 8. (1) Formation of the CTAB-capped seeds by reduction of $HAuCl_4$ with $NaBH_4$, which further grow in solution, thanks to the reaction of $HAuCl_4$ with HQ, giving $AuCl_2^-$ supply. The seeds continue to grow until a symmetry breaking event occurs, leading to {100} and {110} facets. (2) Anisotropic growth of the gold nuclei due to preferential binding of the $C_{19}H_{42}NAgBr_2$ complex on the {110} facets and continuous supply of $AuCl_2^-$. Capping of the {110} facets is represented in red. (3) Competition between growth ({100} facets in ochre) and termination steps ({100} facets in blue) based on the concentrations in the presence of BQ, CTAB, Ag^+, and $AuCl_2^-$. Adapted from ref 28. Copyright 2006 American Chemical Society.

consistent with the discussion in the previous section, with H^+ and $AuCl_4^-$ ions having a negative impact on both the $AuCl_2^-$ and Au^0 formation. Conversely, when the HQ concentration is set at its highest value (19.8 mM), the $HAuCl_4$ concentration no longer has any influence on the gold NRs growth (Figure 7B). This can be explained by the large excess of HQ that has been engaged over $HAuCl_4$ (27:2−990:2), the theoretical stoichiometric ratio being 3:2 for HQ/$HAuCl_4$.[42] It can therefore be assumed that whatever the amount of $HAuCl_4$ added, the impact of its concentration on the concentration of $AuCl_2^-$ produced will be negligible.

In contrast, when the $HAuCl_4$ concentration is set at its lowest value (0.5 mM), increasing the HQ concentration decreases the AR of the obtained gold NRs (Figure 7C). This can be explained by the fact that the growth regime is dictated by the oxidation product of HQ, namely benzoquinone (BQ), which is known to act as a capping agent.[41,42] The latter can also be obtained by reaction with oxygen present in the solution, which at low $HAuCl_4$ concentrations could also become a significant contribution. For this reason, it is likely that the BQ produced competes with rod growth by capping the {100} facets.

To prove the mentioned effect of HQ at low $HAuCl_4$ concentration, 3 experiments varying only the HQ concentration were conducted. These experiments, visible in Figures S7 and S8, clearly show that the predicted and observed results point toward the same trend: increasing the HQ concentration induces a smaller λ_2. Therefore, this experimentally observed trend supports the benzoquinone capping hypothesis.[41,42]

On the other hand, when the concentration of $HAuCl_4$ is set at its highest value (0.7 mM), increasing the HQ concentration increases the AR of the obtained gold NRs (Figure 7D). In this case, sufficient $HAuCl_4$ is engaged to avoid competition between $AuCl_2^-$ ions and BQ for access to the {100} facets. This means that increasing the amount of HQ allows more and more $AuCl_2^-$ ions to be formed, thus favoring NR growth over termination.

Big Picture. Taken together, the above discussions enable us to propose an overall mechanism for the growth of rods based on both the trends already discussed in the literature and those derived from the statistical model developed in this work (Figure 8).

(1) First, small gold nuclei are formed by the reaction of $HAuCl_4$ with $NaBH_4$. These seeds are then poured into the growth solution containing CTAB, $HAuCl_4$, HQ, and $AgNO_3$. By reaction of $HAuCl_4$ with HQ, Au (I) is formed in the solution in the form of $[AuCl_{2-x}Br_x]^-$ anions (noted $AuCl_2^-$ on Figure 8 for simplicity), which can be reduced to Au (0) on the surface of the gold seeds. Above a certain size, symmetry breaking occurs, giving an anisotropic structure to the growing seeds with {100} and {110} facets.

(2) Then, as the complex formed between Ag^+ and CTAB ($C_{19}H_{42}NAgBr_2$) binds preferentially on the {110} facets, only the {100} facets are free for gold deposition, leading to nanoparticles with a rod morphology.

(3) The competition between the growth and termination steps is affected by multiple factors:

(i) The amount of CTAB and $AgNO_3$ is related to the amount of $C_{19}H_{42}NAgBr_2$ formed in solution. Indeed, this study highlighted for both compounds the positive and negative impact on the final AR at low and high regime of concentrations, respectively. At low regime, the more the complex is formed, the more the {110} facets are blocked, the higher the AR. At high regime, the more the complex is formed, the more the competition between the blocking of the {110} and {100} facets exists and the lower the AR. Furthermore, at high concentrations of $AgNO_3$, UPD of Ag^+ becomes significant and at high concentrations of CTAB, CTAB micelles increase in amount, which tends to decrease the selectivity of the blocking of the {110} vs the {100} facets.

(ii) The amount of HQ and $HAuCl_4$: The reduction of $HAuCl_4$ by HQ (giving the $AuCl_2^-$ anions) is pH-dependent and therefore impacted by the amount of $HAuCl_4$ engaged due to its acidic properties.

https://doi.org/10.1021/acs.langmuir.5c00326
Langmuir 2025, 41, 15805−15818

Also, at low concentrations of $HAuCl_4$, the oxidation product of HQ (BQ) competes significantly with the gold deposition on the {100} facets by acting as a capping agent.

CONCLUSIONS

In this work, we developed a DOE to model the parameters involved in the synthesis of gold nanorods (NRs). It provided a better understanding of how to fine-tune their AR by building a model linking their optical property to variations in the concentrations of gold nanoparticle seeds, silver, CTAB, hydroquinone, and $HAuCl_4$. Silver and CTAB were shown to have a significant impact on the optical response and morphology of the resulting rods. In addition, the concentration of gold precursor and hydroquinone can also modify the AR. Among all of the factors modulating the AR of the NRs formed, $HAuCl_4$ concentration seems to be the best option, given the linear relationship linking it to AR. Furthermore, the developed model has been successfully tested and validated, thanks to the match observed in most cases between the prediction interval and the observed values for the position of the λ_2 plasmon band measured by UV−vis spectroscopy for Au NRs synthesized by our group as well as other research groups. This model is available as a web application (https://sites.uclouvain.be/cascados/) for direct and inverse prediction of λ_2. It is recommended to use it to simulate several experiments giving the required λ_2 and then select the one offering the most favorable conditions (concentrations in CTAB and $AgNO_3$ not too high). Moreover, the nanorods obtained showed very good stability, even after one year, thanks to workup by centrifugation and refrigerated storage.

At the same time, the results obtained with DOE have led to a better understanding of rod formation. Many trends already reported in the literature for gold nanorod synthesis were validated by the established model, and new ones were discovered. In particular, the negative impact of the $C_{19}H_{42}NAgBr_2$ complex on AR at high concentrations as well as the intricate pH-dependent interaction between $HAuCl_4$ and HQ, which is highly dependent on the concentrations of both partners. This work also constitutes a statistical confirmation of the formation of a complex between silver and CTAB over a wide concentrations range. The development of this statistical model provides a practical tool for better control of the synthesis of gold NRs and could be applied to other nanoparticle syntheses. Controlling shape, composition, anisotropy, and yield at the nanoscale can be tricky and still relies heavily on "trial and error" developments. Design of experiments helps to optimize synthetic methodologies, unravel the subtle interplay of various experimental conditions, hold predictive value, and allow us to obtain the optimized product. Though, this is rarely done in nanochemistry and nanomaterials elaboration.

ASSOCIATED CONTENT

Supporting Information

The Supporting Information is available free of charge at https://pubs.acs.org/doi/10.1021/acs.langmuir.5c00326.

Additional UV−vis and TEM characterizations (PDF)

AUTHOR INFORMATION

Corresponding Authors

Sophie Madeleine Demoustier-Champagne − *Institute of Condensed Matter and Nanosciences (BSMA Division), UCLouvain, 1348 Louvain-la-Neuve, Belgium;* orcid.org/0000-0003-3045-6060; Email: sophie.demoustier@uclouvain.be

Sophie Hermans − *Institute of Condensed Matter and Nanosciences (MOST Division), UCLouvain, 1348 Louvain-la-Neuve, Belgium;* orcid.org/0000-0003-4715-7964; Email: sophie.hermans@uclouvain.be

Authors

Antonin Engel − *Institute of Condensed Matter and Nanosciences (MOST Division), UCLouvain, 1348 Louvain-la-Neuve, Belgium; Institute of Condensed Matter and Nanosciences (BSMA Division), UCLouvain, 1348 Louvain-la-Neuve, Belgium;* orcid.org/0009-0009-0742-1434

Fabien Drault − *Labiris, Sustainable Chemistry, B-1070 Brussels, Belgium*

Complete contact information is available at: https://pubs.acs.org/10.1021/acs.langmuir.5c00326

Author Contributions

The manuscript was written through contributions of all authors. All authors have given approval to the final version of the manuscript.

Notes

The authors declare no competing financial interest.

ACKNOWLEDGMENTS

Funding from UCLouvain is greatly acknowledged, especially for the teaching assistant position hold by A.E. This work was supported by an ARC Funding grant (CaScadOS project no 21/26-117) from Fédération Wallonie-Bruxelles (Belgium). The authors also thank warmly J.-F. Statsyns for technical assistance and Alessia Tonelli for some of the TEM images. This research has benefitted from the statistical consulting service of Catherine Rasse from the Statistical Methodology and Computing Service, technological platform at UCLouvain—SMCS/LIDAM, UCLouvain.

REFERENCES

(1) Zheng, J.; Cheng, X.; Zhang, H.; Bai, X.; Ai, R.; Shao, L.; Wang, J. Gold nanorods: the most versatile plasmonic nanoparticles. *Chem. Rev.* **2021**, *121* (21), 13342−13453.

(2) Araujo, T. P.; Quiroz, J.; Barbosa, E. C.; Camargo, P. H. Understanding plasmonic catalysis with controlled nanomaterials based on catalytic and plasmonic metals. *COCIS* **2019**, *39*, 110−122.

(3) Zhao, J.; Nguyen, S. C.; Ye, R.; Ye, B.; Weller, H.; Somorjai, G. A.; Alivisatos, A. P.; Toste, F. D. A comparison of photocatalytic activities of gold nanoparticles following plasmonic and interband excitation and a strategy for harnessing interband hot carriers for solution phase photocatalysis. *ACS Cent. Sci.* **2017**, *3* (5), 482−488.

(4) Verma, P.; Kuwahara, Y.; Mori, K.; Yamashita, H. Pd/Ag and Pd/Au bimetallic nanocatalysts on mesoporous silica for plasmon-mediated enhanced catalytic activity under visible light irradiation. *J. Mater. Chem. A* **2016**, *4* (26), 10142−10150.

(5) Ringe, E.; Langille, M. R.; Sohn, K.; Zhang, J.; Huang, J.; Mirkin, C. A.; Van Duyne, R. P.; Marks, L. D. Plasmon length: a universal parameter to describe size effects in gold nanoparticles. *J. Phys. Chem. Lett.* **2012**, *3* (11), 1479−1483.

(6) Turkevich, J.; Stevenson, P. C.; Hillier, J. A study of the nucleation and growth processes in the synthesis of colloidal gold. *Discuss. Faraday Soc.* **1951**, *11*, 55−75.

(7) Sun, Z.; Umar, A.; Zeng, J.; Luo, X.; Song, L.; Zhang, Z.; Chen, Z.; Li, J.; Su, F.; Huang, Y. Highly Pure Gold Nanotriangles with almost 100% Yield for Surface-Enhanced Raman Scattering. *ACS Appl. Nano Mater.* **2022**, *5* (1), 1220−1231.

(8) Pazos-Perez, N.; Guerrini, L.; Alvarez-Puebla, R. A. Plasmon tunability of gold nanostars at the tip apexes. *ACS Omega* **2018**, *3* (12), 17173−17179.
(9) Jana, N. R.; Gearheart, L.; Murphy, C. J. Wet chemical synthesis of high aspect ratio cylindrical gold nanorods. *J. Phys. Chem. B* **2001**, *105* (19), 4065−4067.
(10) Vigderman, L.; Zubarev, E. R. High-yield synthesis of gold nanorods with longitudinal SPR peak greater than 1200 nm using hydroquinone as a reducing agent. *Chem. Mater.* **2013**, *25* (8), 1450−1457.
(11) Huang, X.; Neretina, S.; El-Sayed, M. A. Gold nanorods: from synthesis and properties to biological and biomedical applications. *Adv. Mater.* **2009**, *21* (48), 4880−4910.
(12) Guo, Y.; Thérien-Aubin, H. Nanofibrous photocatalytic membranes based on tailored anisotropic gold/ceria nanoparticles. *ACS Appl. Mater. Interfaces* **2021**, *13* (31), 37578−37588.
(13) Chandrasekhar, P.; Parashar, P. K.; Swami, S. K.; Dutta, V.; Komarala, V. K. Enhancement of Y123 dye-sensitized solar cell performance using plasmonic gold nanorods. *Phys. Chem. Chem. Phys.* **2018**, *20* (14), 9651−9658.
(14) Wu, Y.; Bi, W.; Shi, Z.; Zhuang, X.; Song, Z.; Liu, S.; Chen, C.; Xu, L.; Dai, Q.; Song, H. Unraveling the Dual-Functional Mechanism of Light Absorption and Hole Transport of Cu2Cd x Zn1−x SnS4 for Achieving Efficient and Stable Perovskite Solar Cells. *ACS Appl. Mater. Interfaces* **2020**, *12* (15), 17509−17518.
(15) Cho, S. H.; Kim, W. H.; Lee, S. M.; Choi, K. C. 7.4: AC Plasma Displays with Gold Nanorods in the Protecting Layer. *SID Int. Symp. Dig. Technol. Pap* **2012**, *43* (1), 68−70.
(16) Greybush, N. J.; Charipar, K.; Geldmeier, J. A.; Bauman, S. J.; Johns, P.; Naciri, J.; Charipar, N.; Park, K.; Vaia, R. A.; Fontana, J. Dynamic plasmonic pixels. *ACS Nano* **2019**, *13* (4), 3875−3883.
(17) Kesharwani, P.; Ma, R.; Sang, L.; Fatima, M.; Sheikh, A.; Abourehab, M. A.; Gupta, N.; Chen, Z.-S.; Zhou, Y. Gold nanoparticles and gold nanorods in the landscape of cancer therapy. *Mol. Cancer* **2023**, *22* (1), 98.
(18) Abadeer, N. S.; Murphy, C. J. Recent progress in cancer thermal therapy using gold nanoparticles. *Nanomater. Neoplasms* **2021**, 143−217.
(19) Pellas, V.; Hu, D.; Mazouzi, Y.; Mimoun, Y.; Blanchard, J.; Guibert, C.; Salmain, M.; Boujday, S. Gold nanorods for LSPR biosensing: synthesis, coating by silica, and bioanalytical applications. *Biosensors* **2020**, *10* (10), 146.
(20) Chen, Y.-S.; Zhao, Y.; Yoon, S. J.; Gambhir, S. S.; Emelianov, S. Miniature gold nanorods for photoacoustic molecular imaging in the second near-infrared optical window. *Nat. Nanotechnol.* **2019**, *14* (5), 465−472.
(21) Li, P.; Wu, Y.; Li, D.; Su, X.; Luo, C.; Wang, Y.; Hu, J.; Li, G.; Jiang, H.; Zhang, W. Seed-mediated synthesis of tunable-aspect-ratio gold nanorods for near-infrared photoacoustic imaging. *Nanoscale Res. Lett.* **2018**, *13* (1), 313.
(22) Jana, N. R.; Gearheart, L.; Murphy, C. J. Seed-mediated growth approach for shape-controlled synthesis of spheroidal and rod-like gold nanoparticles using a surfactant template. *Adv. Mater.* **2001**, *13* (18), 1389−1393.
(23) Grzelczak, M.; Pérez-Juste, J.; Mulvaney, P.; Liz-Marzán, L. M. Shape control in gold nanoparticle synthesis. In *Colloidal Synthesis of Plasmonic Nanometals*; Jenny Stanford Publishing, 2020; pp 197−220.
(24) Zhao, J.; Wang, J.; Brock, A. J.; Zhu, H. Plasmonic heterogeneous catalysis for organic transformations. *J. Photochem. Photobiol., C* **2022**, *52*, 100539.
(25) Su, G.; Yang, C.; Zhu, J.-J. Fabrication of gold nanorods with tunable longitudinal surface plasmon resonance peaks by reductive dopamine. *Langmuir* **2015**, *31* (2), 817−823.
(26) Ye, X.; Zheng, C.; Chen, J.; Gao, Y.; Murray, C. B. Using binary surfactant mixtures to simultaneously improve the dimensional tunability and monodispersity in the seeded growth of gold nanorods. *Nano Lett.* **2013**, *13* (2), 765−771.
(27) Luo, X.; Wang, X.; Zhang, L.; Song, L.; Sun, Z.; Zhao, Y.; Su, F.; Huang, Y. Engineering miniature gold nanorods with tailorable plasmonic wavelength in NIR region via ternary surfactants mediated growth. *Nano Res.* **2023**, *16* (4), 5087−5097.
(28) Orendorff, C. J.; Murphy, C. J. Quantitation of metal content in the silver-assisted growth of gold nanorods. *J. Phys. Chem. B* **2006**, *110* (9), 3990−3994.
(29) Yoo, S.; Youn, G.; Lee, H.; Kwon, J. S.; Lee, Y.; Lee, S. Synthesis of ultra-small gold nanorods: Effect of reducing agent on reaction rate control. *Bull. Korean Chem. Soc.* **2023**, *44* (8), 648−652.
(30) Nikoobakht, B.; El-Sayed, M. A. Preparation and growth mechanism of gold nanorods (NRs) using seed-mediated growth method. *Chem. Mater.* **2003**, *15* (10), 1957−1962.
(31) Morasso, C.; Picciolini, S.; Schiumarini, D.; Mehn, D.; Ojea-Jiménez, I.; Zanchetta, G.; Vanna, R.; Bedoni, M.; Prosperi, D.; Gramatica, F. Control of size and aspect ratio in hydroquinone-based synthesis of gold nanorods. *J. Nanoparticle Res.* **2015**, *17*, 330.
(32) Ward, C. J.; Tronndorf, R.; Eustes, A. S.; Auad, M. L.; Davis, E. W. Seed-mediated growth of gold nanorods: limits of length to diameter ratio control. *J. Nanomater.* **2014**, *2014*, 47.
(33) Pérez-Juste, J.; Liz-Marzán, L. M.; Carnie, S.; Chan, D. Y.; Mulvaney, P. Electric-field-directed growth of gold nanorods in aqueous surfactant solutions. *Adv. Funct. Mater.* **2004**, *14* (6), 571−579.
(34) Ye, X.; Gao, Y.; Chen, J.; Reifsnyder, D. C.; Zheng, C.; Murray, C. B. Seeded growth of monodisperse gold nanorods using bromide-free surfactant mixtures. *Nano Lett.* **2013**, *13* (5), 2163−2171.
(35) Hormozi-Nezhad, M. R.; Robatjazi, H.; Jalali-Heravi, M. Thorough tuning of the aspect ratio of gold nanorods using response surface methodology. *Anal. Chim. Acta* **2013**, *779*, 14−21.
(36) Burrows, N. D.; Harvey, S.; Idesis, F. A.; Murphy, C. J. Understanding the seed-mediated growth of gold nanorods through a fractional factorial design of experiments. *Langmuir* **2017**, *33* (8), 1891−1907.
(37) Rao, A.; Grzelczak, M. Revisiting El-Sayed Synthesis: Bayesian Optimization for Revealing New Insights during the Growth of Gold Nanorods. *Chem. Mater.* **2024**, *36* (5), 2577−2587.
(38) Gleason, S. P.; Dahl, J. C.; Elzouka, M.; Wang, X.; Byrne, D. O.; Cho, H.; Gababa, M.; Prasher, R. S.; Lubner, S.; Chan, E. M.; et al. Automated Gold Nanorod Spectral Morphology Analysis Pipeline. *ACS Nano* **2024**, *18* (51), 34646−34655.
(39) Moses, O. A.; Adam, M. L.; Chen, Z.; Ezeh, C. I.; Huang, H.; Wang, Z.; Wang, Z.; Wang, B.; Li, W.; Wang, C.; et al. Machine learning and robot-assisted synthesis of diverse gold nanorods via seedless approach. *Artif. Intell. Chem.* **2023**, *1* (2), 100028.
(40) Liu, X.-H.; Luo, X.-H.; Lu, S.-X.; Zhang, J.-C.; Cao, W.-L. A novel cetyltrimethyl ammonium silver bromide complex and silver bromide nanoparticles obtained by the surfactant counterion. *J. Colloid Interface Sci.* **2007**, *307* (1), 94−100.
(41) Amatori, S.; Lopez, A.; Meneghini, C.; Calcabrini, A.; Colone, M.; Stringaro, A.; Migani, S.; Khalakhan, I.; Iucci, G.; Venditti, I.; et al. Gold nanorods derivatized with CTAB and hydroquinone or ascorbic acid: spectroscopic investigation of anisotropic nanoparticles of different shapes and sizes. *Nanoscale Adv.* **2023**, *5* (15), 3924−3933.
(42) Sirajuddin; Mechler, A.; Torriero, A. A. J.; Nafady, A.; Lee, C. Y.; Bond, A. M.; O'Mullane, A. P.; Bhargava, S. K. The formation of gold nanoparticles using hydroquinone as a reducing agent through a localized pH change upon addition of NaOH to a solution of HAuCl4. *Colloids Surf. A: Physicochem. Eng. Asp.* **2010**, *370* (1−3), 35−41.
(43) Picciolini, S.; Mehn, D.; Ojea-Jiménez, I.; Gramatica, F.; Morasso, C. Hydroquinone based synthesis of gold nanorods. *J. Vis. Exp.* **2016**, No. e54319.
(44) Jessl, S.; Tebbe, M.; Guerrini, L.; Fery, A.; Alvarez-Puebla, R. A.; Pazos-Perez, N. Silver-Assisted Synthesis of Gold Nanorods: the Relation between Silver Additive and Iodide Impurities. *Small* **2018**, *14* (20), 1703879.
(45) Xu, Y.; Chen, L.; Ye, X.; Wang, X.; Yu, J.; Zhao, Y.; Cao, M.; Xia, Z.; Sun, B.; Zhang, Q. Cooperative interactions among CTA+, Br−and Ag+ during seeded growth of gold nanorods. *Nano Res.* **2017**, *10*, 2146−2155.

https://doi.org/10.1021/acs.langmuir.5c00326
Langmuir 2025, 41, 15805−15818

(46) Scarabelli, L.; Sánchez-Iglesias, A.; Pérez-Juste, J.; Liz-Marzán, L. M. A "Tips and Tricks" Practical Guide to the Synthesis of Gold Nanorods. *J. Phys. Chem. Lett.* **2015**, *6* (121), 4270−4279.
(47) Liu, M.; Guyot-Sionnest, P. Mechanism of silver (I)-assisted growth of gold nanorods and bipyramids. *J. Phys. Chem. B* **2005**, *109* (47), 22192−22200.
(48) Wang, Z.; Gao, R.; Nikoobakht, B.; El-Sayed, M. Surface reconstruction of the unstable {110} surface in gold nanorods. *J. Phys. Chem. B* **2000**, *104* (23), 5417−5420.
(49) Chang, H.-H.; Murphy, C. J. Mini gold nanorods with tunable plasmonic peaks beyond 1000 nm. *Chem. Mater.* **2018**, *30* (4), 1427−1435.
(50) Murphy, C. J.; Thompson, L. B.; Alkilany, A. M.; Sisco, P. N.; Boulos, S. P.; Sivapalan, S. T.; Yang, J. A.; Chernak, D. J.; Huang, J. The many faces of gold nanorods. *J. Phys. Chem. Lett.* **2010**, *1* (19), 2867−2875.
(51) Hubert, F.; Testard, F.; Spalla, O. Cetyltrimethylammonium bromide silver bromide complex as the capping agent of gold nanorods. *Langmuir* **2008**, *24* (17), 9219−9222.
(52) Rodríguez-Fernández, J.; Pérez-Juste, J.; Mulvaney, P.; Liz-Marzán, L. M. Spatially-directed oxidation of gold nanoparticles by Au (III)− CTAB complexes. *T J. Phys. Chem. B* **2005**, *109* (30), 14257−14261.
(53) Edgar, J. A.; McDonagh, A. M.; Cortie, M. B. Formation of gold nanorods by a stochastic "popcorn" mechanism. *ACS Nano* **2012**, *6* (2), 1116−1125.

https://doi.org/10.1021/acs.langmuir.5c00326
Langmuir 2025, 41, 15805−15818